Chemosphere 291 (2022) 133002

Contents lists available at ScienceDirect

Chemosphere

journal homepage: www.elsevier.com/locate/chemosphere

Bentonite-based sodium alginate/ dextrin cross-linked poly (acrylic acid) hydrogel nanohybrids for facile removal of paraquat herbicide from aqueous solutions

Sourbh Thakur [a,b,**], Ankit Verma [b], Pankaj Raizada [b], Oguzhan Gunduz [c], Dawid Janas [a], Walaa F. Alsanie [d], Fabrizio Scarpa [e], Vijay Kumar Thakur [f,g,h,*]

[a] Department of Organic Chemistry, Bioorganic Chemistry and Biotechnology, Silesian University of Technology, B. Krzywoustego 4, 44-100, Gliwice, Poland
[b] School of Advanced Chemical Sciences, Shoolini University, Solan, 173229, Himachal Pradesh, India
[c] Center for Nanotechnology & Biomaterials Application and Research, Marmara University, Istanbul, Turkey
[d] Department of Clinical Laboratories Sciences, The Faculty of Applied Medical Sciences, Taif University, P.O. Box 11099, Taif, 21944, Saudi Arabia
[e] Bristol Composites Institute, University of Bristol, Bristol, BS8 1TR, UK
[f] Biorefining and Advanced Materials Research Center, SRUC, EH9 3JG, UK
[g] Department of Mechanical Engineering, School of Engineering, Shiv Nadar University, Uttar Pradesh, 201314, India
[h] School of Engineering, University of Petroleum & Energy Studies (UPES), Dehradun, 248007, Uttarakhand, India

HIGHLIGHTS

- Paraquat herbicide accumulation in environment is an emerging problem across the world.
- Sodium alginate (SAlg), dextrin and acrylic acid (PAA) based biopolymeric hydrogel network was successfully designed.
- Bentonite was incorporated in SAlg/ dextrin-cl-PAA matrix to produce SAlg/ dextrin-cl-PAA/bentonite.
- SAlg/dextrin-cl-PAA/bentonite showed high adsorption of paraquat herbicide.
- SAlg/dextrin-cl-PAA/bentonite can be reused effectively for up to six paraquat adsorption-desorption cycles.

GRAPHICAL ABSTRACT

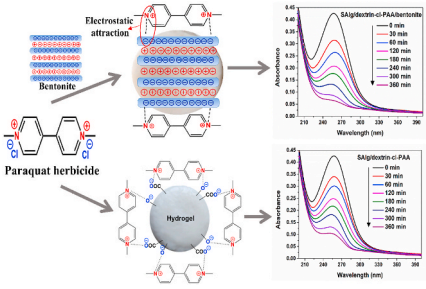

ARTICLE INFO

Handling Editor: Hafiz M.N. Iqbal

Keywords:
Sodium alginate
Dextrin
Bentonite
Hydrogel composite
Paraquat removal

ABSTRACT

Removal of hazardous herbicides from the aqueous solution is critical for overcoming health-related issues across the wider population. In the current work, we have prepared sodium alginate (SAlg), dextrin, and acrylic acid (AA) based cross-linked hydrogels, composed of bentonite incorporated in the biocompatible hydrogel matrix. This hydrogel composite can remove highly toxic herbicide paraquat (PQ). As-synthesised hydrogel (SAlg/ dextrin-cl-PAA) and hydrogel composite (SAlg/dextrin-cl-PAA/bentonite) were further analysed by infra-red spectroscopy (FTIR), X-ray diffraction (XRD), field emission scanning electron microscopy (FESEM) and thermogravimetric analysis (TGA/DSC). For the first time, PQ adsorption onto sodium and dextrin-based hydrogel

* Corresponding author. Biorefining and Advanced Materials Research Center, SRUC, EH9 3JG, UK.
** Corresponding author. Department of Organic Chemistry, Bioorganic Chemistry and Biotechnology, Silesian University of Technology, B. Krzywoustego 4, 44-100, Gliwice, Poland.
E-mail addresses: Sourbh.Thakur@polsl.pl, thakursourbh@gmail.com (S. Thakur), vijay.thakur@sruc.ac.uk (V.K. Thakur).

https://doi.org/10.1016/j.chemosphere.2021.133002
Received 11 September 2021; Received in revised form 8 November 2021; Accepted 18 November 2021
Available online 26 November 2021

was also evaluated. The measured highest removal capacities were 76.923 and 90.909 mg g^{-1} for the SAlg/dextrin-cl-PAA and SAlg/dextrin-cl-PAA/bentonite, respectively. Pseudo-second-order (PSO) and Langmuir isotherm models have shown to be best suited for accurately describing the adsorption mechanism. A thermodynamics study verified that the adsorption of PQ on adsorbents is spontaneous, favourable and exothermic. Moreover, reusability analysis shows that the adsorbents possess good reproducibility even after six successive cycles. The adsorption results demonstrate that the synthesised adsorbents are very efficient for removing herbicides (PQ) from wastewater.

1. Introduction

Pesticides and herbicides are the most indispensable part of modern agriculture for the protection of crops and livestock (Ashvinder K. Rana et al., 2021b). Pesticides are a vast category of organic pollutants, which can be mainly classified as organochlorine pesticides (Gupta and Gupta, 2017), organonitrogen pesticides (Fodor-Csorba, 1998), organophosphorus pesticides (Mileson, 2014), herbicides (Gupta, 2011) and fungicides (Doble and Kumar, 2005), etc. There is no doubt that synthetic pesticides have resulted in substantial economic benefits over the past few decades and provided support for agricultural production and increased crop protection. However, they have some serious health consequences related to all living beings (Ates et al., 2020; Dwivedi et al., 2014; Mugni et al., 2012; Ashvinder K. Rana et al., 2021a).

Paraquat (PQ) is a non-selective bipyridine herbicide also known as methyl viologen; Fig. 1 illustrates the chemical structure of paraquat dichloride. Initially, paraquat was synthesised by Widel and Russian (Leite et al., 2013). It was first used as a herbicide at rubber farms in Malaysia and has since become widespread. PQ is an anti-contact herbicide that suppresses photosynthesis and kills plants. (Santos et al., 2011). This material is mainly used for weed control for the cultivation of cocoa or coffee. The quick action of PQ, even in small quantities, explains its widespread utilisation. It results in less soil degradation and lowers costs compared to the majority of herbicides. Unfortunately, PQ is toxic to humans when swallowed. It causes damage to the digestive tract, kidneys, and lungs. PQ is a highly toxic agent that should not exceed a dosage rate of 35 mg kg^{-1} in humans (Danish et al., 2010). In different countries like Taiwan and New Zealand, the established maximum contamination standard of 10 μg L^{-1} or 0.01 mg L^{-1} for drinking water has been fixed by the government (Duncanson et al., 2000; Tsai and Lai, 2006).

There are two reported remediation procedures for removing PQ in water and wastewater. i.e. oxidation and adsorption of PQ on the porous materials (Leite et al., 2013). The first case includes the process of oxidation of the PQ, which degrades the pollutant structure. To do this, different reagents are combined, often in the presence of UV light, which generates intensely reactive free radicals (Leite et al., 2013). The pinpoint drawback of this process is the production of toxins as side products when decomposition does not work in favourable conditions (Leite et al., 2013). In the second approach, PQ can be adsorbed on the porous surface. Particularly, hydrogels have the influential ability to adsorb this pollutant to enable its degradation at the speedy rate at an affordable cost (Aouada et al., 2009). In the past decades, hydrogels have been extensively used for the adsorption of pollutants from aqueous solutions (Thakur et al., 2018, 2022). Such a gel with a three-dimensional, cross-linked network and exceptional ability to take the maximum amount of aqueous fluids and water is naturally suited for such an application (Thakur and Thakur, 2015). The presence of hydrophilic groups within the hydrogel matrix contributes to the high potential for swelling. (Ashvinder Kumar Rana et al., 2021; Sharma et al., 2020a; Thakur and Voicu, 2016), which further enhances the capability of the material for pollutant interception.

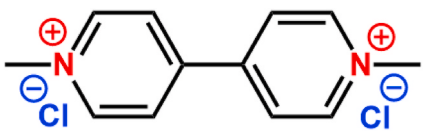

Fig. 1. Chemical structure of paraquat dichloride (PQ).

Sodium alginate (SAlg) is a natural linear polysaccharide derived from the cell wall of brown algae. It can absorb quantities of water through hydrogels due to its interesting structure; SAlg contains –COOH groups that can dissociate in the aqueous medium and produce negative charges. Dextrin is an affordable polysaccharide utilised in the food and textile sectors; a low-molecular-weight polysaccharide made up of D-glucose units linked together by alpha-(1 → 4) or alpha-(1 → 6) glycoside linkages. Bentonite is a clay mineral made up mostly of montmorillonite; two layers of the oxygen-silicon tetrahedron are sandwiched between two layers of alumina octahedral sheet in its 2:1 crystal structure (Ali et al., 2020). The expansion, absorption and caking characteristics of this clay are excellent.

Yue et al. synthesised sodium alginate and polyacrylamide based hydrogel through in situ polymerisation using nanoclay, carbon nanotube and nano-silica (Yue et al., 2019). The reported highest adsorption of Cu(II) by sodium alginate/polyacrylamide/carbon nanotube hydrogel was 46 mg g^{-1}. The sodium alginate/polyacrylic acid hydrogel and sodium alginate/polyacrylic acid/ZnO hydrogel nanocomposites were prepared by Makhado et al. (2020). The maximum methylene blue adsorption capacity of sodium alginate/polyacrylic acid hydrogel and sodium alginate/polyacrylic acid/ZnO hydrogel nanocomposites were 1129 mg g^{-1} and 1529.6 mg g^{-1} respectively. Pashaei-Fakhri et al. prepared the hydrogel (sodium alginate/acrylamide) and hydrogel nanocomposite (sodium alginate/acrylamide/graphene oxide) by the free radical copolymerisation method (Pashaei-Fakhri et al., 2021). The achieved maximum adsorption capacity for crystal violet dye adsorption was 62.07 mg g^{-1} and 100 30 mg g^{-1} using hydrogel (sodium alginate/acrylamide) and hydrogel nanocomposite (sodium alginate/acrylamide/graphene oxide), respectively.

The current work aims to examine the capability of hydrogels made of sodium alginate (SAlg), dextrin, poly (acrylic acid) (PAA) and bentonite for removing paraquat dichloride. The influence of the amount of bentonite, the pH of the PQ solution and adsorbents dosage on PQ adsorption and recyclability was studied. A UV–vis spectrophotometer was used to test the batch adsorption sample for paraquat. Additionally, isotherm and kinetic models and thermodynamic analysis were used to describe the sorption process. Furthermore, swelling analysis was used to design sodium alginate/dextrin-cl-poly (acrylic acid) (SAlg/dextrin-cl-PAA) and sodium alginate/dextrin-cl-poly (acrylic acid)/bentonite (SAlg/dextrin-cl-PAA/bentonite).

2. Experimental

2.1. Materials

Sodium alginate (SAlg), ($C_6H_9NaO_7$, 216.12 g mol^{-1}), acrylic acid (AA), ($C_3H_4O_2$, 72.06 g mol^{-1}), white dextrin, (($(C_6H_{10}O_5)n.$ × H_2O, 180.156 g mol^{-1}), potassium persulphate (KSO; $K_2S_2O_8$, 270.3 g, 98 percent) and N, N′-methylene bisacrylamide (MBA; $C_7H_{10}N_2O_2$, 154.17 g mol^{-1}) and bentonite powder were purchased from LOBA CHEMIE PVT. LTD, India. The chemicals were used directly without any refinement.

2.2. Synthesis of SAlg/dextrin-cl-PAA

The free-radical copolymerisation technique synthesised the SAlg/dextrin-cl-PAA. The desired amount of dextrin and SAlg were dissolved in a 100 mL beaker containing 1.6×10^{-2} L double distilled water. The mass ratios of dextrin and SAlg are given in Table S1. After the proper mixing, KSO was added to the aqueous dextrin/SAlg, followed by the sequential addition of PAA and MBA. The solution was uniformly mixed and treated under microwave to produce SAlg/dextrin-cl-PAA. After allowing the prepared SAlg/dextrin-cl-PAA to cool to room temperature, it was washed several times with acetone to extract homopolymers. Finally, sample granules were dried for 48 h at 50 °C. The various reaction conditions were designed to achieve optimal swelling results, as demonstrated in Table S2. The schematic representation for the synthesis procedure is given in Fig. 2.

2.3. Synthesis of SAlg/dextrin-cl-PAA/bentonite

The free-radical copolymerisation technique has also allowed to synthesise the SAlg/dextrin-cl-PAA/bentonite. In this experiment, SAlg and dextrin were used as a backbone, KSO as initiator, AA as a monomer, MBA as cross-linker, and bentonite clay as a filler. For the preparation of bentonite clay loaded SAlg/dextrin-cl-PAA/bentonite, bentonite clay was dispersed in 1.6×10^{-2} L of double-distilled water, which was used instead of pure water. The same manufacturing procedure was followed as described in the case of SAlg/dextrin-cl-PAA. The amount of bentonite clay was optimized to reach the appropriate swelling percentage of SAlg/dextrin-cl-PAA/bentonite, as shown in Table S3.

2.4. Water retention study

The water-holding efficiency of the SAlg/dextrin-cl-PAA and SAlg/dextrin-cl-PAA/bentonite were analysed by the free swelling method (Feng et al., 2014). For 20 h, a pre-weighed sample was placed in 0.15 L double-distilled water at a temperature of 25 °C. After that, the swollen piece was taken out of the water, its surface was wiped, and weighed. The water-holding efficiency of the prepared samples was calculated using Equation (1).

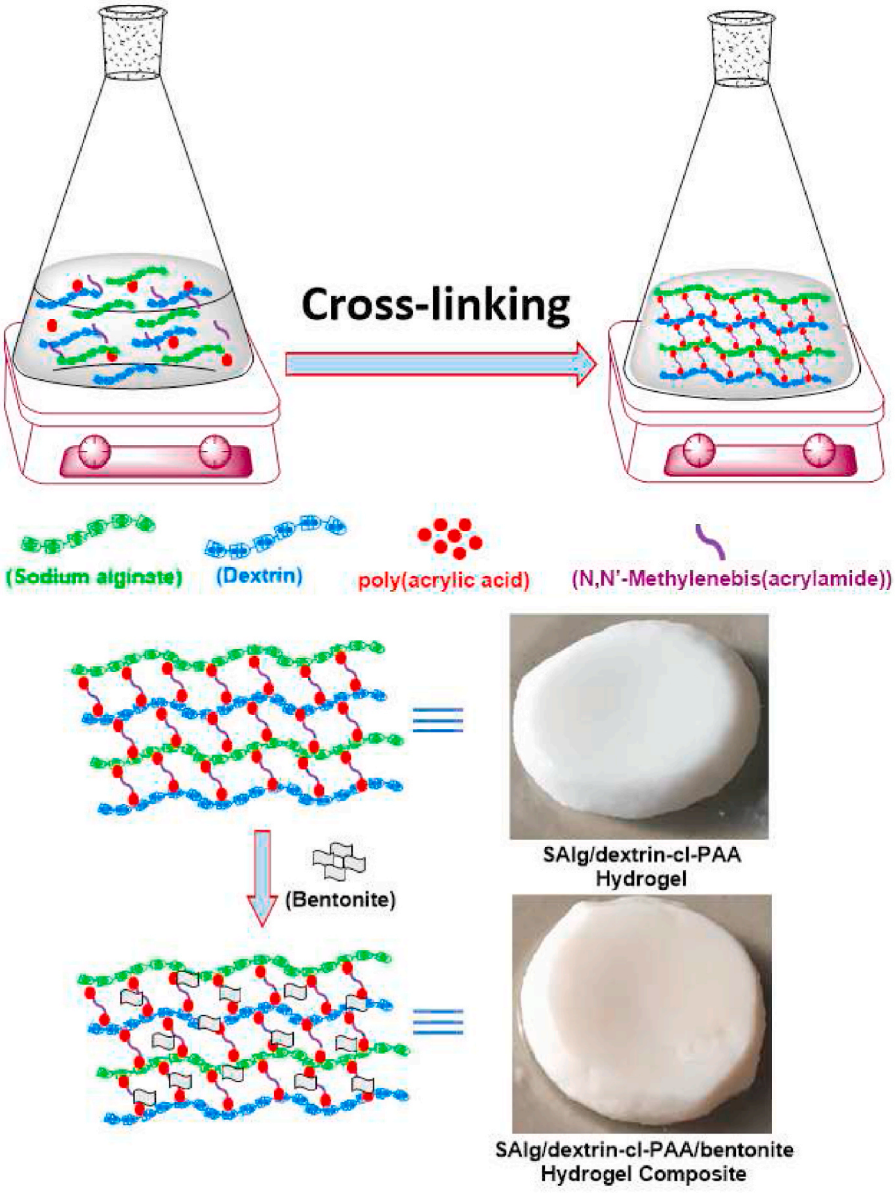

Fig. 2. Schematic representation of the synthesis of SAlg/dextrin-cl-PAA and SAlg/dextrin-cl-PAA/bentonite.

$$\text{Swelling } \% = \frac{W_s - W_d}{W_d} \times 100 \quad (1)$$

$\frac{W_s-W_d}{W_d} \times 100 \frac{W_s-W_d}{W_d} \times 100 \frac{W_s-W_d}{W_d} \times 100 \frac{W_s-W_d}{W_d} \times 100 \frac{W_s-W_d}{W_d} \times 100 \frac{W_s-W_d}{W_d} \times 100 \frac{W_s-W_d}{W_d} \times 100$where W_s and W_d are weights of swollen SAlg/dextrin-cl-PAA and dry SAlg/dextrin-cl-PAA, respectively.

2.5. Adsorption of PQ

PQ adsorption was analysed by batch experiments using SAlg/dextrin-cl-PAA and SAlg/dextrin-cl-PAA/bentonite (Hosseinzadeh and Abdi, 2017). Using double-distilled water, a 1000 ppm solution of PQ was formed. A known amount ($2 \times 10^{-2} - 10 \times 10^{-2}$ g) of the prepared samples (SAlg/dextrin-cl-PAA and SAlg/dextrin-cl-PAA/bentonite) were placed in 0.02 L of 20 mg L^{-1} PQ solution. The amount of PQ adsorption was measured by the absorbance of residual PQ solution with the help of a UV–Vis spectrophotometer at wavelength 257 nm. The PQ removal percentage was determined using Equation (2):

$$\text{Adsorption percentage} = \frac{C_0 - C_e}{C_e} \times 100 \quad (2)$$

The PQ adsorbed per unit mass of adsorbent (Q_e) was measured using Equation (3):

$$Q_e = \frac{(C_o - C_e)V}{M} \times 100 \quad (3)$$

Where, C_e and C_o denote the equilibrium and initial concentrations, V represents the volume of the PQ solution in litres (L), and M denotes the adsorbent weight in grams (g).

2.6. Reusability of SAlg/dextrin-cl-PAA and SAlg/dextrin-cl-PAA/bentonite

The reusability of SAlg/dextrin-cl-PAA and SAlg/dextrin-cl-PAA/bentonite were examined with the help of six successive sorption cycles. For these analyses, 6 × 10-2 g of SAlg/dextrin-cl-PAA, and SAlg/dextrin-cl-PAA/bentonite were placed into 0.02 L of 20 mg L^{-1} PQ solution at pH 7 and agitated for 320 min. After that, adsorbed SAlg/dextrin-cl-PAA and SAlg/dextrin-cl-PAA/bentonite were dispersed into 0.05 L of 0.01 N HCl and stirred for 120 min; the recovered SAlg/dextrin-cl-PAA and SAlg/dextrin-cl-PAA/bentonite were dried and utilised for adsorption of PQ.

2.7. Characterisation

The FTIR spectra were recorded in the wavelength range 4000–400 cm^{-1} using an FTIR spectrophotometer (L1600312 spectrum TWOLITA/ZnSe) (Agilent Technologies, Santa Clara, CA, USA). FESEM images were acquired using Nova Nano SEM-450 FESEM (JFEI Hillsboro, OR, USA). X-ray diffraction (XRD) spectra were obtained in the 2°–80° range using a SmartLab 9 kW rotating anode X-ray diffractometer at a scanning rate of 1° min^{-1} (Rigaku Corporation, Tokyo, Japan). TGA/DSC were performed in a nitrogen atmosphere (flow rate 20 mL min^{-1}) on a NETZSCH Geratebau GmbH (Wittelsbacherstraβe 42, 95,100 Selb, Germany) (Model: STA 449 F1 jupiter) at a heating rate of 10 °C min^{-1} between 20 and 1000 °C.

3. Result and discussion

3.1. Optimisation of swelling for the synthesis of SAlg/dextrin-cl-PAA and SAlg/dextrin-cl-PAA/bentonite

3.1.1. SAlg: dextrin ratio

As shown in Table S1, the SAlg: dextrin ratio was investigated to determine the swelling percentage (%) of the synthesised SAlg/dextrin-cl-PAA. The swelling percentage improved as the amount of SAlg increased, reaching a maximum at SAlg: dextrin ratio of 8:1. The increase in swelling percentage was attributed to the hydrophilic character of SAlg. The increase of its content, therefore, promoted water adsorption by the material.

3.1.2. Initiator (KSO) concentration

The effect of initiator concentration (0.5×10^{-2} - 2.0×10^{-2} mol L^{-1}) on SAlg/dextrin-cl-PAA swelling was investigated (Table S2). The maximum swelling percentage was observed to be 982.15% at a KSO concentration of 0.9×10^{-2} mol L^{-1}. The excess free radical active sites led to the homo-polymerisation reaction (Feng et al., 2014), and hence the swelling percentage was reduced at KSO concentration beyond 0.9×10^{-2} mol L^{-1}. In this case, the hydrogel was unable to develop an appropriate 3D structure.

3.1.3. Reaction time

SAlg/dextrin-cl-PAA swelling was influenced by reaction time (40s – 80s) (Table S2). The swelling percentage was enhanced when the time was increased from 40s to 60s. It reached maximum swelling percentage at the 60s, and after that, it decreased. Beyond the 60s, excessive formation of branched chains took place, which could be entangled, thereby inhibiting the polymer structure's growth. Hence, SAlg/dextrin-cl-PAA could not hold the water molecules as well, which was indicated by the declined swelling percentage from the 60s–80s reaction time.

3.1.4. Solvent volume

The swelling percentage of SAlg/dextrin-cl-PAA was analysed using solvent volumes from 1×10^{-2} L to 2.2×10^{-2} L (Table S2). The maximum swelling percentage (1339.34%) was obtained at 1.6×10^{-2} L. The swelling percentage was enhanced up to 1.6×10^{-2} L and then started to decrease. Due to hydroxyl radical formation through water, polymerisation propagation and swelling percentage were enhanced from 1×10^{-2} L to 1.6×10^{-2} L. At high solvent volumes (>1.6×10^{-2} L), the concentration of monomer, initiator, and cross-linker was decreased, which slowed down the copolymerisation reaction, and hence the swelling percentage was reduced (Chen et al., 2009).

3.1.5. pH

SAlg/dextrin-cl-PAA was sensitive to the pH environment. The swelling percentage of SAlg/dextrin-cl-PAA was analysed at various pH values (1.0–13.0) (Table S2). Under acidic conditions, carboxylate groups were protonated, so the anion - anion ($COO^- - COO^-$) group's repulsive force were decreased. Therefore swelling percentage was reduced in the acidic medium (Bao et al., 2011). Conversely, in primary conditions, ionised carboxylic groups led to increasing the electrostatic repulsion. Consequently, the maximum swelling percentage (1584.8%) was observed at pH 10. At higher pH (>10), however, the swelling percentage of SAlg/dextrin-cl-PAA decreased due to excess Na + ions responsible for the charge screening effect. It inhibited the anion - anion ($COO^- - COO^-$) group's repulsion (Hua and Wang, 2009).

3.1.6. Microwave power

The influence of microwave power (20% - 100%) on the SAlg/dextrin-cl-PAA swelling was also evaluated (Table S2). At 40% microwave power, 1696.84% was the highest swelling percentage. The initial increase in the swelling percentage with the increase in microwave power from 20% to 40% was due to a fast radical and cross-linking reaction. However, at high microwave power (>40%), the swelling percentage was decreased due to the annihilation of the 3D structure of SAlg/dextrin-cl-PAA (Bao et al., 2011). Therefore, in this work, the microwave power was maintained at 40% throughout the synthesis of SAlg/dextrin-cl-PAA.

3.1.7. Monomer concentration

Different acrylic acid monomer (AA) concentrations (0.45 mol L^{-1} – 2.27 mol L^{-1}) were studied to observe the swelling percentage of SAlg/dextrin-cl-PAA (Table S2). The swelling percentage was increased from 1545.6% to 1825.8% for 0.45–1.36 mol L^{-1}, respectively. Increased AA concentrations (>1.36 mol L^{-1}) resulted in the SAlg/dextrin-cl-PAA matrix self-cross-linking and hardening, which was manifested by low SAlg/dextrin-cl-PAA swelling percentage (Thakur and Arotiba, n. d.).

3.1.8. Cross-linker concentration

Various cross-linker concentrations (0.6×10^{-2} - 2.2×10^{-2} mol L^{-1}) were analysed to determine the swelling percentage of SAlg/dextrin-cl-PAA, and the results are presented in Table S2. The maximum swelling percentage (1998.47%) was obtained at 1.01×10^{-2} mol L^{-1}. Owing to the high cross-linking density of SAlg/dextrin-cl-PAA at concentrations greater than 1.01×10^{-2} mol L^{-1}, the free space between the SAlg/dextrin-cl-PAA hydrogel polymeric chains decreased, attributed to the reduced water-holding capacity of SAlg/dextrin-cl-PAA (Sharma et al., 2020b).

3.1.9. Bentonite amount

The swelling percentage of SAlg/dextrin-cl-PAA/bentonite depends on amounts of bentonite (Table S3). At 4×10^{-2} g of bentonite, a higher swelling percentage of 2518.36% was reported for SAlg/dextrin-cl-PAA/bentonite. Beyond 4×10^{-2} g of bentonite, the swelling percentage of SAlg/dextrin-cl-PAA/bentonite was reduced because excess of bentonite increased the cross-linking density and decreased the hydrophilicity of SAlg/dextrin-cl-PAA/bentonite. Therefore, 4×10^{-2} gm of bentonite was used in SAlg/dextrin-cl-PAA/bentonite for further experimental studies.

3.2. Characterisation

3.2.1. FT-IR

Fig. 3 illustrates FT-IR spectra of SAlg, dextrin, bentonite, SAlg/dextrin-cl-PAA, and SAlg/dextrin-cl-PAA/bentonite. The prominent peaks around 3426 cm^{-1} and 3292 cm^{-1} in the SAlg and dextrin spectra were related to the stretching modes of the OH groups, while the minor peaks at 2917 and 2896 cm^{-1} resulted from the C–H stretching vibrations (Das et al., 2015; Zare et al., 2018). Peaks 1638 and 1409 cm^{-1} were attributed to COO^- and C–C bending vibrations, respectively. The peak at 1030 cm^{-1} confirmed the presence of C–O stretching, while the peak 883 cm^{-1} was due to the linkage of mannuronic and guluronic units. The C–*O*–C stretching vibration mode corresponded to peaks at 1004, 1092 and 1138 cm^{-1} (Aprilliza, 2017).

The bentonite spectrum revealed peaks at 3623 and 3395 cm^{-1} ascribed to the interlayer and intralayer H-bonded O–H stretching, respectively. A peak at 1631 cm^{-1} was indicative of bending of H–*O*–H (Zaitan et al., 2008). Peaks at 516 and 456 cm^{-1} were ascribed to Si–O bending; another peak at 904 cm^{-1} was attributed to the Al–Al–OH bond. In addition, the peak at 681 cm^{-1} was identified as belonging to the vibration of Al–OH (Atkovska et al., 2016; Hristodor et al., 2012).

In SAlg/dextrin-cl-PAA and SAlg/dextrin-cl-PAA/bentonite, a broad peak at 1545 cm^{-1} emerged because of the amide stretching vibration of the cross-linker. Carboxylic groups were stretched at 1706 and 1452 cm^{-1}, which indicated a successful AA grafting. Lastly, the peaks at 529 and 465 cm^{-1} for SAlg/dextrin-cl-PAA/bentonite were due to the Si–O bending, which verified the effective incorporation of bentonite in the hydrogel. (Hua and Wang, 2009; Thakur and Arotiba, n. d.).

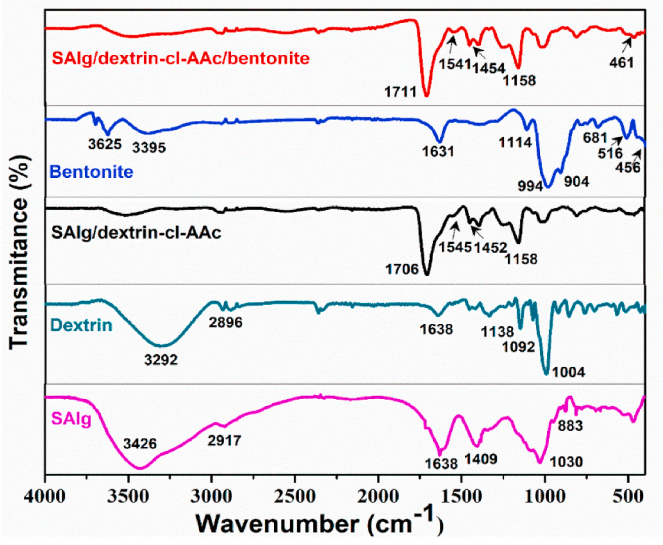

Fig. 3. FT-IR spectra of SAlg, dextrin, SAlg/dextrin-cl-PAA, bentonite and SAlg/dextrin-cl-PAA/bentonite (wavenumbers of the main features are indicated in the figure).

3.2.2. X-ray diffraction (XRD)

XRD patterns of SAlg, dextrin, SAlg/dextrin-cl-PAA, bentonite, and SAlg/dextrin-cl-PAA/bentonite are displayed in Fig. 4. The weak broad peak around 22.21° in SAlg was ascribed to the low crystallinity of the material (Aprilliza, 2017). In the dextrin patterns, peaks at 15.09°, 16.97°, 17.82°, and 22.95° clearly indicated the presence of a semi-crystalline behaviour (Mittal et al., 2016). The broadness of the peak was enhanced in the SAlg/dextrin-cl-PAA, which confirmed the contribution from the grafting of the PAA (Hua and Wang, 2009). The XRD patterns of clay (bentonite) showed the presence of intense peaks at 6.99°, 19.7°, 20.8°, and 26.6° (Zare and Lakouraj, 2014). The broad peak at 6.99° corresponded to the (001) diffraction plane of a layered structure (JCPDS file Number: 03–0019) (Mishra et al., 2018). The peak at 26.6° (210) showed the existence of quartz in bentonite (JCPDS file Number: 01-083-2466) (Mishra et al., 2018). The broadness in XRD patterns related to SAlg/dextrin-cl-PAA/bentonite demonstrated the uniform dispersion of the bentonite in SAlg/dextrin-cl-PAA hydrogel.

3.2.3. Morphology analysis

The surface morphology of SAlg, dextrin, bentonite, SAlg/dextrin-cl-PAA and SAlg/dextrin-cl-PAA/bentonite was analysed by FE-SEM. SAlg had an even and regular surface (Figure S1a), while dextrin showed granular morphology (Figure S1b). SAlg/dextrin-cl-PAA, on the other hand, featured a rough surface and wrinkled structure (Fig. 5a and b).

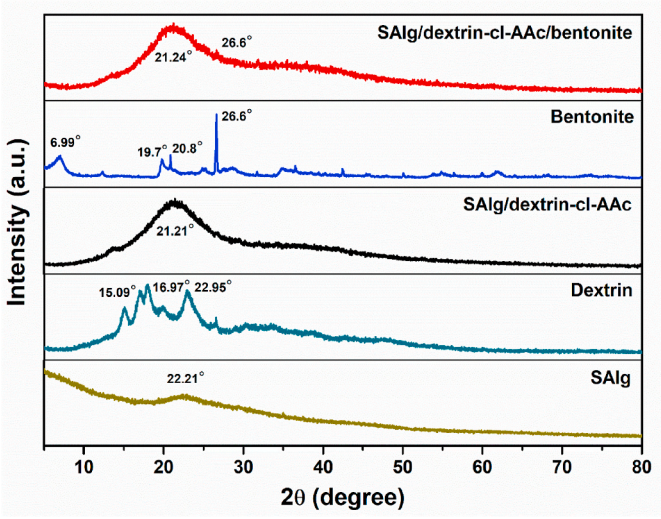

Fig. 4. XRD patterns of SAlg, dextrin, SAlg/dextrin-cl-PAA, bentonite, and SAlg/dextrin-cl-PAA/bentonite.

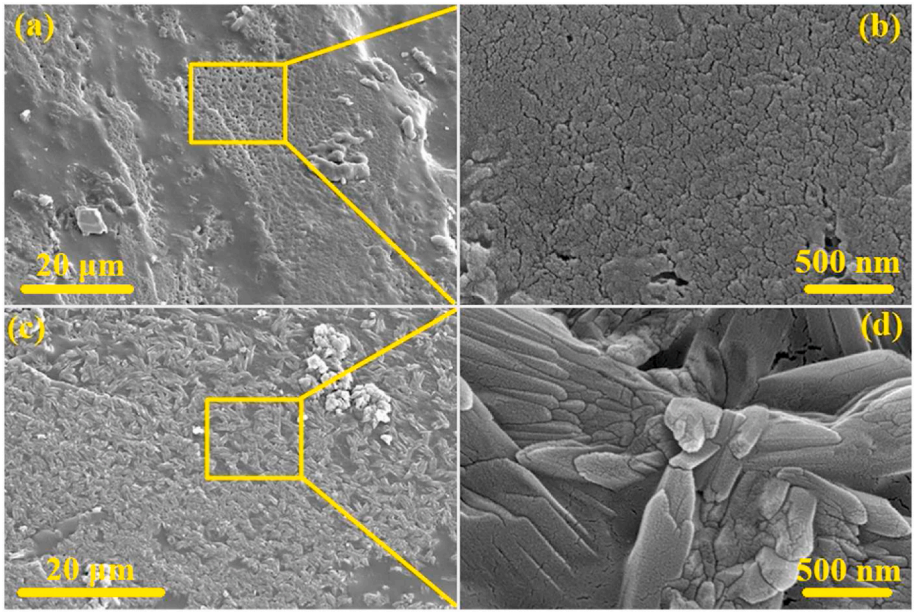

Fig. 5. FESEM micrographs of **(a,b)** SAlg/dextrin-cl-PAA and **(c,d)** SAlg/dextrin-cl-PAA/bentonite.

Furthermore, bentonite demonstrated sheet-like nature, with a fine lamellar structure (Figure S1c). Consequently, the roughness of SAlg/dextrin-cl-PAA increased after the dispersion of bentonite in the SAlg/dextrin-cl-PAA matrix. This resulted in the composite hydrogel material's rough and sheet-like morphology (Fig. 5c and d).

3.2.4. TGA/DSC

The TGA/DSC curves of SAlg/dextrin-cl-PAA and SAlg/dextrin-cl-PAA/bentonite are shown in Fig. 6. The initial weight loss stage in the temperature range of 20–179.6 °C, was attributed to the removing of water molecules trapped in the samples. The second stage of weight loss between 179.6 °C to 277.8 °C corresponded to the disintegration of glycosidic bonds and the decomposition of the alginate and dextrin backbone (Mittal et al., 2016; Thakur and Arotiba, 2018). The final decomposition temperatures were 539.4 °C and 602.5 °C for SAlg/dextrin-cl-PAA and SAlg/dextrin-cl-PAA/bentonite correspondingly, hence the dispersion of the bentonite increases the thermal stability of SAlg/dextrin-cl-PAA. Moreover, DSC analysis was used to examine the transition temperatures of SAlg/dextrin-cl-PAA and SAlg/dextrin-cl-PAA/bentonite. Endothermic peaks at 252.8 °C and 218.1 °C for SAlg/dextrin-cl-PAA and SAlg/dextrin-cl-PAA/bentonite, respectively, were associated with the degradation temperature of a backbone made of SAlg and dextrin (Zare et al., 2014). Exothermic peaks were also present at 481.8 °C and 498.1 °C for SAlg/dextrin-cl-PAA and SAlg/dextrin-cl-PAA/bentonite correspondingly. Those peaks were related to the decomposition of the remaining components of the specimens (Zare et al., 2014).

3.3. Adsorption of PQ by SAlg/dextrin-cl-PAA and SAlg/dextrin-cl-PAA/bentonite

SAlg/dextrin-cl-PAA and SAlg/dextrin-cl-PAA/bentonite were investigated for the adsorption of the toxic herbicide (PQ). A representation of the mechanisms behind the interactions between SAlg/dextrin-cl-PAA and PQ is shown in Fig. 7. The SAlg/dextrin-cl-PAA and PQ have different surface charges, so the electrostatic interaction is responsible for the PQ adsorption onto SAlg/dextrin-cl-PAA. (Verma et al., 2020). The bentonite clay's reported pH point zero charge (pHpzc) value was 6.2 (Nwosu et al., 2018), so the bentonite surface possesses a negative charge at pH 7. Hence, the goal of this study was to validate whether incorporating bentonite in SAlg/dextrin-cl-PAA matrix would enhance

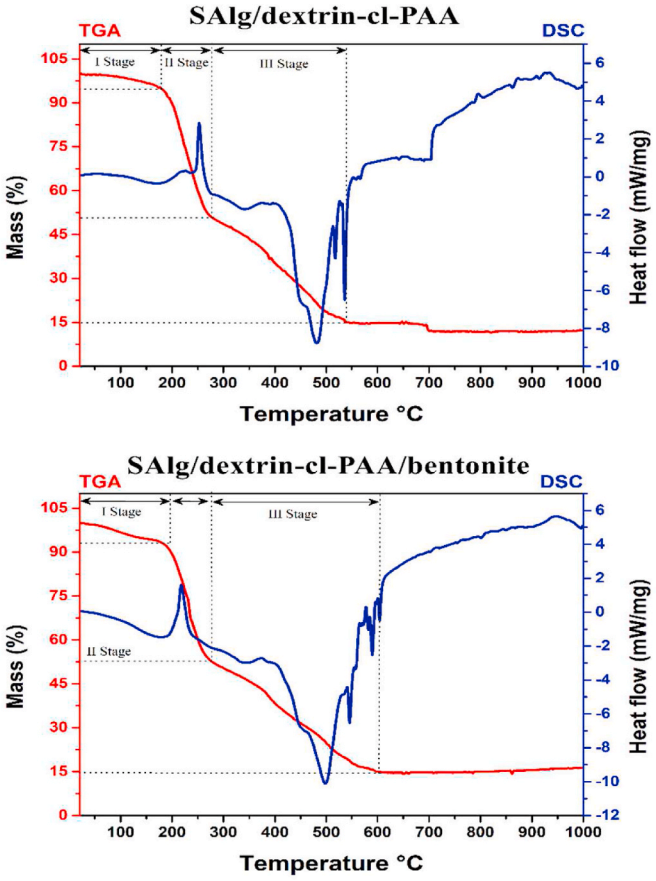

Fig. 6. TGA/DSC curves of **(a)** SAlg/dextrin-cl-PAA and **(b)** SAlg/dextrin-cl-PAA/bentonite.

the anionic behaviour, thereby increasing the PQ adsorption capacity of SAlg/dextrin-cl-PAA.

3.3.1. Influence of bentonite dose on PQ adsorption

The quantity of bentonite clay in SAlg/dextrin-cl-PAA/bentonite was

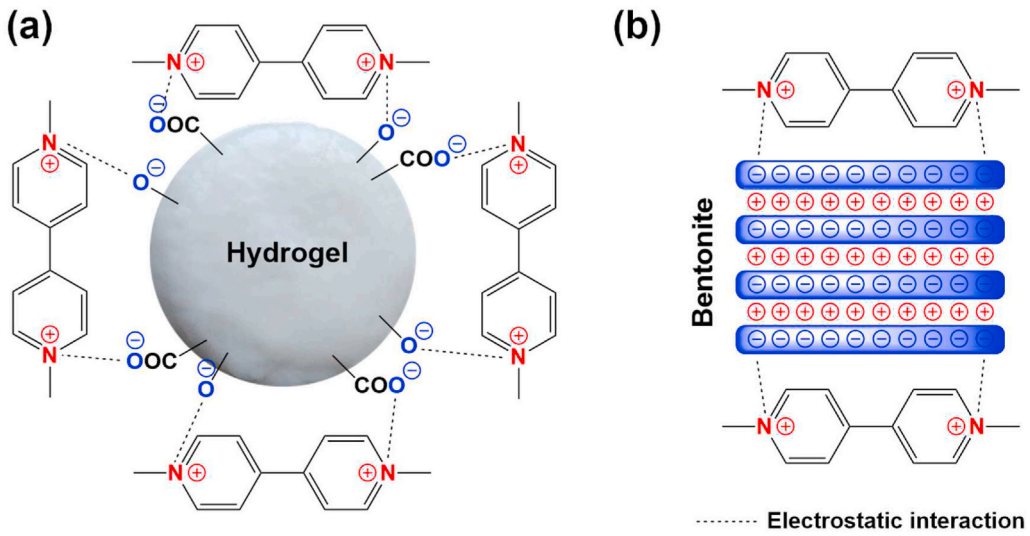

Fig. 7. Plausible interactions between SAlg/dextrin-cl-PAA, bentonite and PQ.

varied between 2×10^{-2} g and 8×10^{-2} g (Fig. 8a). The percentage of PQ adsorption increased from 54.5% to 65.6% when the quantity of bentonite was increased from 2×10^{-2} to 4×10^{-2} g, respectively. The reported maximum PQ adsorption percentage was 65.6% at the bentonite amount of 4×10^{-2} g. The incorporation of bentonite in SAlg/dextrin-cl-PAA attributed to more PQ adsorption. Bentonite having negative charge potential on the lattice surface (Tahir and Rauf, 2006) led to an increase in the anionic character of the SAlg/dextrin-cl-PAA/bentonite. The SAlg/dextrin-cl-PAA/bentonite had therefore an improved PQ adsorption than the SAlg/dextrin-cl-PAA. The PQ adsorption percentage started to decrease beyond 4×10^{-2} g of bentonite. Due to the excess bentonite, the three-dimensional structure of the SAlg/dextrin-cl-PAA/bentonite became distorted, lowering the percentage of PQ adsorption.

3.3.2. *Influence of pH on PQ adsorption*

The role of pH (1–13) in PQ adsorption was examined (Fig. 8b). Point zero charge (pH_{PZC}) is an important measurement that shows the value

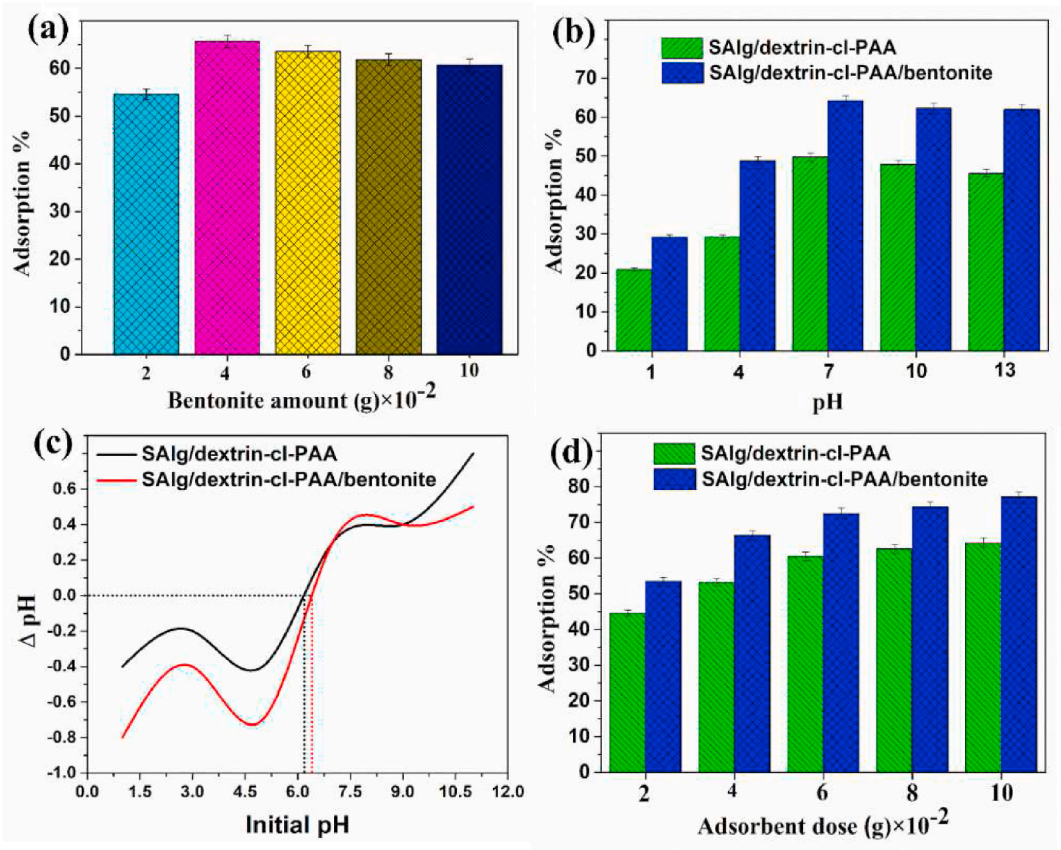

Fig. 8. Effect of **(a)** bentonite dose, **(b)** pH and **(c)** point zero charge **(d)** SAlg/dextrin-cl-PAA and SAlg/dextrin-cl-PAA/bentonite adsorbents dose on PQ adsorption percentage.

of the pH at which the adsorbent surface is free of charge. In the present study, pH_{PZC} values were 6.1 and 6.4 for the SAlg/dextrin-cl-PAA and the SAlg/dextrin-cl-PAA/bentonite, respectively (Fig. 8c). At acidic pH, SAlg/dextrin-cl-PAA and SAlg/dextrin-cl-PAA/bentonite showed a low adsorption percentage, while the adsorption of PQ was high at the basic pH level. The adsorption of PQ on the SAlg/dextrin-cl-PAA and the SAlg/dextrin-cl-PAA/bentonite hydrogels was not efficient under acidic conditions ($pH < pH_{PZC}$), because of the protonation of the functional groups in SAlg/dextrin-cl-PAA and SAlg/dextrin-cl-PAA/bentonite. Additionally, the adsorption was reduced in acidic environments. In contrast, SAlg/dextrin-cl-PAA and the SAlg/dextrin-cl-PAA/bentonite at $pH > pH_{PZC}$ exhibited negative charge through deprotonation of the functional group in the SAlg/dextrin-cl-PAA and SAlg/dextrin-cl-PAA/bentonite. This resulted in a high PQ adsorption through electrostatic interactions. The presence of the COO^- groups at basic pH provided the SAlg/dextrin-cl-PAA and SAlg/dextrin-cl-PAA/bentonite adsorbents an anionic character, which explained the high percentage of PQ adsorption. Nevertheless, the excess sodium ions at pH 13 screened the carboxylate ion from the PQ and led to a slight decrease in the percentage of PQ adsorption (Huang et al., 2019).

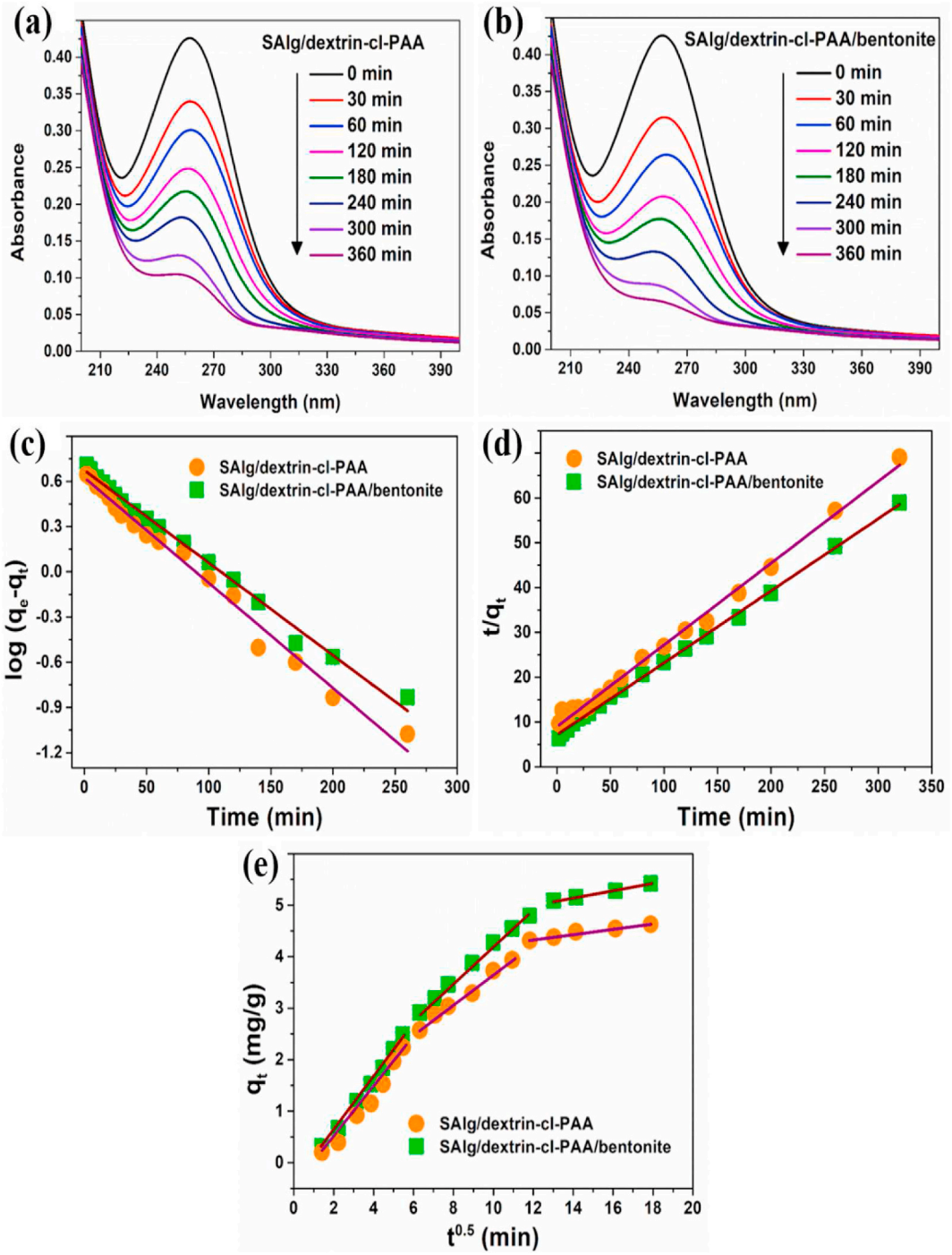

Fig. 9. UV–vis absorption spectra of PQ by **(a)** SAlg/dextrin-cl-PAA and **(b)** SAlg/dextrin-cl-PAA/bentonite, **(c)** pseudo-first, **(d)** pseudo-second and **(e)** intra-particle diffusion for PQ adsorption onto SAlg/dextrin-cl-PAA and SAlg/dextrin-cl-PAA/bentonite.

3.3.3. Influence of adsorbent dose

The impact of different adsorbent dosages (2×10^{-2} g to 10×10^{-2} g) on the removal of PQ herbicide is shown in Fig. 8d. With an increase in the dose of adsorbents (SAlg/dextrin-cl-PAA and SAlg/dextrin-cl-PAA/bentonite) from 2×10^{-2} g to 6×10^{-2} g, a successively increase in the adsorption percentage was observed. For 2×10^{-2} g and 10×10^{-2} g adsorbent doses, the percentages of PQ adsorption onto SAlg/dextrin-cl-PAA/bentonite were 53.5% and 77%, respectively. In contrast, in the case of SAlg/dextrin-cl-PAA, PQ adsorption percentages were 44.5% and 64.2% correspondingly. The increase in adsorption with increasing amounts of adsorbent were ascribed to a rise in the number of binding sites available for binding the PQ (Makhado et al., 2018).

3.3.4. Adsorption kinetics

The PQ adsorption kinetics on SAlg/dextrin-cl-PAA and SAlg/dextrin-cl-PAA/bentonite were measured by fitting pseudo-first (PFO), pseudo-second-order (PSO) and intra-particle diffusion (IPD) kinetics (see supporting information). The time-dependent UV–vis absorption spectra of the PQ herbicide is shown in Fig. 9a and b. The decrease in PQ absorbance with time confirmed the successful adsorption capabilities of PQ by the SAlg/dextrin-cl-PAA and SAlg/dextrin-cl-PAA/bentonite. The fitted data for the PFO, PSO and IPD models are shown in Fig. 9c–e, while the measured parameters are shown in Table S4.

SAlg/dextrin-cl-PAA and SAlg/dextrin-cl-PAA/bentonite had PSO kinetic correlation coefficients (R^2) 0.994 and 0.998. The high correlation coefficient (R^2) values for PSO kinetics explained that it suited better PQ adsorption than the PFO kinetics model. The graph in Fig. 9e illustrates the intra-particle diffusion (IPD) model, divided into three linear parts. The first linear region represented the surface penetration due to the large surface area of the adsorbents; the presence of a second linear region demonstrated the presence of intra-particle diffusion of the PQ, while the third linear region was representative of the final equilibrium phase for the adsorption of PQ on SAlg/dextrin-cl-PAA and SAlg/dextrin-cl-PAA/bentonite. PQ molecules were stuck by intra-particle diffusion in the inner pores of SAlg/dextrin-cl-PAA and SAlg/dextrin-cl-PAA/bentonite (Mahlangu et al., 2019). Thus, the adsorption of PQ onto SAlg/dextrin-cl-PAA and SAlg/dextrin-cl-PAA/bentonite was caused by intra-particle and external mass-diffusion processes.

3.3.5. Adsorption isotherm

The adsorption isotherms for the PQ adsorption were determined at different temperatures (25, 35, and 45 °C). The experimental data for the PQ adsorption were fitted using two isotherm models: Langmuir (Figure S2a,b) and Freundlich (Figure S2c,d) (see supporting information). The PQ adsorptions on SAlg/dextrin-cl-PAA and SAlg/dextrin-cl-PAA/bentonite were better fitted by the Langmuir isotherm model due to their high correlation coefficient value. Table S5 contains the measured correlation coefficients (R^2) and isotherm parameters. The maximum adsorption tendency of SAlg/dextrin-cl-PAA and SAlg/dextrin-cl-PAA/bentonite were 76.92 mg g^{-1} and 90.90 mg g^{-1}. The tendency by SAlg/dextrin-cl-PAA and SAlg/dextrin-cl-PAA/bentonite of removing PQ decreased with the temperature, indicating that the PQ adsorption was exothermic (Mahlangu et al., 2019). Also, R_L values between 0 and 1 showed that the PQ adsorption was suited for the Langmuir isotherm model.

3.3.6. Thermodynamics

Thermodynamic data provide information about the spontaneity and energy variations throughout the adsorption procedure. The thermodynamics study was performed by using the Van't Hoff equation (see supplementary information). The calculated results for the PQ adsorption by the SAlg/dextrin-cl-PAA and the SAlg/dextrin-cl-PAA/bentonite are given in Table S6. The ΔG° (Gibbs free energy), ΔH° (enthalpy), and ΔS° (entropy) were analysed using the slope and intercept of the Van't Hoff plot (ln K_d vs 1/T) (Kumar et al., 2018). The negative values of ΔH° (−3.177 and −7.324 kJ mol^{-1} for the PQ adsorption onto SAlg/dextrin-cl-PAA and SAlg/dextrin-cl-PAA/bentonite, respectively) confirmed the exothermic nature of the reaction. The ΔG° negative values also demonstrated the spontaneous nature of the PQ adsorption on SAlg/dextrin-cl-PAA and SAlg/dextrin-cl-PAA/bentonite at various temperatures (318.15, 308.15, and 298.15 K). ΔS° values in the negative range (−9.07 and −15.64) also indicated a stable adsorption mechanism and no improvement in the structure of the solid-liquid interface.

3.4. Reusability of SAlg/dextrin-cl-PAA and SAlg/dextrin-cl-PAA/bentonite

The reusability of adsorbents is important because it has a direct impact on the efficiency and costs of the adsorption. Consequently, we investigated the reusability of SAlg/dextrin-cl-PAA and SAlg/dextrin-cl-PAA/bentonite throughout six adsorption-desorption cycles. Fig. 10 illustrates the percentage of the PQ adsorption on SAlg/dextrin-cl-PAA and SAlg/dextrin-cl-PAA/bentonite over a six-cycles period. The PQ adsorption percentages were 85.6%, 83.9%, 80.3%, 78.3%, 75.7%,73.7% (from the 1st to the 6th cycles, respectively) and 73.0%,70.4%, 68.7%, 65.7%, 62.4% and 59.8% (again, from the 1st to the 6th respective cycles) for SAlg/dextrin-cl-PAA/bentonite and SAlg/dextrin-cl-PAA, respectively. These findings support the reusability of SAlg/dextrin-cl-PAA and SAlg/dextrin-cl-PAA/bentonite for PQ removal, as the decrease of the performance is small and appears to stabilise.

3.5. Adsorption capacity of SAlg/dextrin-cl-PAA and SAlg/dextrin-cl-PAA/bentonite compared with the state of the art

The synthesised sodium alginate/dextrin-cl-poly (acrylic acid) (SAlg/dextrin-cl-PAA) and sodium alginate/dextrin-cl-poly (acrylic acid)/bentonite (SAlg/dextrin-cl-PAA/bentonite) are efficient, and also possess a greater capacity for PQ adsorption than other adsorbents described in open literature (Table S7). The highest removal capacities were 76.923 and 90.909 mg g^{-1} for SAlg/dextrin-cl-PAA and Salg/dextrin-cl-PAA/bentonite, respectively. In light of the results published so far, the proposed solution outperforms other formulations that make use of a wide spectrum of other adsorbents. The high efficiency of the PQ adsorption here is credited to the efficient combination of SAlg, dextrin, poly (acrylic acid) and bentonite.

4. Conclusions

We have successfully developed a bentonite-incorporated SAlg/

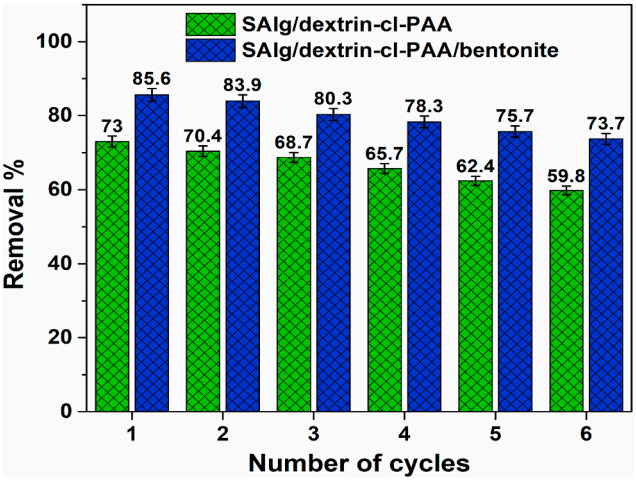

Fig. 10. Recycling ability of SAlg/dextrin-cl-PAA and SAlg/dextrin-cl-PAA/bentonite for PQ removal up to six cycles.

dextrin-cl-PAA adsorbent for efficient interception of paraquat herbicide. The obtained maximum swelling percentage for SAlg/dextrin-cl-PAA/bentonite at optimized synthesis conditions (initiator concentration = 0.9×10^{-2} mol L^{-1}, cross-linker = 1.01×10^{-2} mol L^{-1}, monomer = 1.36 mol L^{-1}, solvent amount = 1.6×10^{-2} L, pH = 10, reaction time = 60 s, microwave power = 40% and bentonite amount = 4×10^{-2} gm) was as high as 2518.36%. The adsorption of the paraquat herbicide (PQ) depends on the amount of bentonite, the pH and doses of adsorbents. Under optimized experimental conditions (bentonite amount = 4×10^{-2} g, PQ solution pH = 7 and adsorbent dose = 6×10^{-2} g), the maximum adsorption tendency of th eSAlg/dextrin-cl-PAA and the SAlg/dextrin-cl-PAA/bentonite were 76.923 and 90.909 mg g^{-1}. The pseudo-second-order (PSO) kinetics and Langmuir isotherm model adequately represented the adsorption of the PQ. SAlg/dextrin-cl-PAA and SAlg/dextrin-cl-PAA/bentonite showed a very consistent reusability for up to six consecutive cycles of PQ adsorption-desorption. Environmentally friendly, cost-effective, and pH-sensitive SAlg/dextrin-cl-PAA/bentonite hydrogels can therefore serve as useful adsorbents for wastewater remediation.

Author statement

Original draft writing: **S.T.**, **A.V.**, **P.R.** Writing, review and editing: Q.G., **D.J.**, **W.A.**, **F.S.**, **V.K.T.** Supervision: **F.S.**, **V.K.T.**

Declaration of competing interest

The authors declare that they have no known competing financial interests or personal relationships that could have appeared to influence the work reported in this paper.

Acknowledgement

Sourbh Thakur would like to thank the Silesian University of Technology, Poland (ID-UB program) for the financial support of the research. Walaa F. Alsanie would like to acknowledge Taif University TURSP program (TURSP-2020/53) for funding. Vijay Kumar Thakur would also like to thank the research support provided by the Royal Academy of Engineering (IAPP18-19\295), and UKIERI (DST/INT/UK/P-164/2017).

Appendix A. Supplementary data

Supplementary data to this article can be found online at https://doi.org/10.1016/j.chemosphere.2021.133002.

References

Ali, S.H., Abbas, A.M., Abdulrazzak, F.H., 2020. Adsorption of heavy metals on bentonite and modified bentonite clay, factors, kinetic and thermodynamic studies/a review. Alg. J. Mat. Chem. 3, 90–106.

Aouada, F.A., Pan, Z., Orts, W.J., Mattoso, L.H., 2009. Removal of paraquat pesticide from aqueous solutions using a novel adsorbent material based on polyacrylamide and methylcellulose hydrogels. J. Appl. Polym. Sci. 114, 2139–2148.

Aprilliza, M., 2017. Characterization and properties of sodium alginate from brown algae used as an ecofriendly superabsorbent. In: IOP Conference Series: Materials Science and Engineering. IOP Publishing, 012019.

Ates, B., Koytepe, S., Ulu, A., Gurses, C., Thakur, V.K., 2020. Chemistry, structures, and advanced applications of nanocomposites from biorenewable resources. Chem. Rev. 120, 9304–9362. https://doi.org/10.1021/acs.chemrev.9b00553.

Atkovska, K., Bliznakovska, B., Ruseska, G., Bogoevski, S., Boskovski, B., Grozdanov, A., 2016. ADSORPTION OF Fe (II) AND Zn (II) IONS FROM LANDFILL LEACHATE BY NATURAL BENTONITE. J. Chem. Technol. Metall. 51.

Bao, Y., Ma, J., Li, N., 2011. Synthesis and swelling behaviors of sodium carboxymethyl cellulose-g-poly (AA-co-AM-co-AMPS)/MMT superabsorbent hydrogel. Carbohydr. Polym. 84, 76–82.

Chen, Y., Liu, Y., Tan, H., Jiang, J., 2009. Synthesis and characterization of a novel superabsorbent polymer of N, O-carboxymethyl chitosan graft copolymerized with vinyl monomers. Carbohydr. Polym. 75, 287–292.

Danish, M., Sulaiman, O., Rafatullah, M., Hashim, R., Ahmad, A., 2010. Kinetics for the removal of paraquat dichloride from aqueous solution by activated date (Phoenix dactylifera) stone carbon. J. Dispersion Sci. Technol. 31, 248–259.

Das, D., Ghosh, P., Dhara, S., Panda, A.B., Pal, S., 2015. Dextrin and poly (acrylic acid)-based biodegradable, non-cytotoxic, chemically cross-linked hydrogel for sustained release of ornidazole and ciprofloxacin. ACS Appl. Mater. Interfaces 7, 4791–4803.

Doble, M., Kumar, A., 2005. Chapter 8 - biodegradation of pesticides. In: Doble, M., Kumar, A. (Eds.), Biotreatment of Industrial Effluents. Butterworth-Heinemann, Burlington, pp. 89–100. https://doi.org/10.1016/B978-075067838-4/50009-9.

Duncanson, M., Russell, N., Weinstein, P., Baker, M., Skelly, C., Hearnden, M., Woodward, A., 2000. Rates of notified cryptosporidiosis and quality of drinking water supplies in Aotearoa, New Zealand. Water Res. 34, 3804–3812.

Dwivedi, C., Gupta, A., Chaudhary, A., Nandi, C.K., 2014. Gold nanoparticle chitosan composite hydrogel beads show efficient removal of methyl parathion from waste water. RSC Adv. 4, 39830–39838.

Feng, D., Bai, B., Ding, C., Wang, H., Suo, Y., 2014. Synthesis and swelling behaviors of yeast-g-poly (acrylic acid) superabsorbent co-polymer. Ind. Eng. Chem. Res. 53, 12760–12769.

Fodor-Csorba, K., 1998. Chapter 18 - pesticides in environmental samples. In: Deyl, Z., Mikšik, I., Tagliaro, F., Tesařová, E. (Eds.), Journal of Chromatography Library, Advanced Chromatographic and Electromigration Methods in BioSciences. Elsevier, pp. 779–831. https://doi.org/10.1016/S0301-4770(08)60316-4.

Gupta, P.K., 2011. Chapter 39 - herbicides and fungicides. In: Gupta, R.C. (Ed.), Reproductive and Developmental Toxicology. Academic Press, San Diego, pp. 503–521. https://doi.org/10.1016/B978-0-12-382032-7.10039-6.

Gupta, R.K., Gupta, R.C., 2017. Chapter 68 - placental toxicity. In: Gupta, R.C. (Ed.), Reproductive and Developmental Toxicology, second ed. Academic Press, pp. 1301–1325. https://doi.org/10.1016/B978-0-12-804239-7.00068-8.

Hosseinzadeh, H., Abdi, K., 2017. Efficient removal of methylene blue using a hybrid organic–inorganic hydrogel nanocomposite adsorbent based on sodium alginate–silicone dioxide. J. Inorg. Organomet. Polym. Mater. 27, 1595–1612.

Hristodor, C.-M., Vrinceanu, N., Pui, A., Novac, O., Copcia, V.-E., Popovici, E., 2012. Textural and morphological characterization of chitosan/bentonite nanocomposite. Environ. Eng. Manag. J. (EEMJ) 11.

Hua, S., Wang, A., 2009. Synthesis, characterization and swelling behaviors of sodium alginate-g-poly (acrylic acid)/sodium humate superabsorbent. Carbohydr. Polym. 75, 79–84.

Huang, C.-F., Tu, C.-W., Lee, R.-H., Yang, C.-H., Hung, W.-C., Andrew Lin, K.-Y., 2019. Study of various diameter and functionality of TEMPO-oxidized cellulose nanofibers on paraquat adsorptions. Polym. Degrad. Stabil. 161, 206–212. https://doi.org/10.1016/j.polymdegradstab.2019.01.023.

Kumar, N., Mittal, H., Alhassan, S.M., Ray, S.S., 2018. Bionanocomposite hydrogel for the adsorption of dye and reusability of generated waste for the photodegradation of ciprofloxacin: a demonstration of the circularity concept for water purification. ACS Sustain. Chem. Eng. 6, 17011–17025.

Leite, M.P., dos Reis, L.G.T., Robaina, N.F., Pacheco, W.F., Cassella, R.J., 2013. Adsorption of paraquat from aqueous medium by Amberlite XAD-2 and XAD-4 resins using dodecylsulfate as counter ion. Chem. Eng. J. 215, 691–698.

Mahlangu, T., Das, R., Abia, L.K., Onyango, M., Ray, S.S., Maity, A., 2019. Thiol-modified magnetic polypyrrole nanocomposite: an effective adsorbent for the adsorption of silver ions from aqueous solution and subsequent water disinfection by silver-laden nanocomposite. Chem. Eng. J. 360, 423–434.

Makhado, E., Pandey, S., Modibane, K.D., Kang, M., Hato, M.J., 2020. Sequestration of methylene blue dye using sodium alginate poly (acrylic acid)@ ZnO hydrogel nanocomposite: kinetic, isotherm, and thermodynamic investigations. Int. J. Biol. Macromol. 162, 60–73.

Makhado, E., Pandey, S., Nomngongo, P.N., Ramontja, J., 2018. Preparation and characterization of xanthan gum-cl-poly (acrylic acid)/o-MWCNTs hydrogel nanocomposite as highly effective re-useable adsorbent for removal of methylene blue from aqueous solutions. J. Colloid Interface Sci. 513, 700–714.

Mileson, B.E., 2014. Common mechanism of toxicity in pesticides. In: Wexler, P. (Ed.), Encyclopedia of Toxicology, third ed. Academic Press, Oxford, pp. 1024–1025. https://doi.org/10.1016/B978-0-12-386454-3.00117-2.

Mishra, A., Mehta, A., Kainth, S., Basu, S., 2018. Effect of g-C3N4 loading on TiO2/Bentonite nanocomposites for efficient heterogeneous photocatalytic degradation of industrial dye under visible light. J. Alloys Compd. 764, 406–415.

Mittal, A., Ahmad, R., Hasan, I., 2016. Iron oxide-impregnated dextrin nanocomposite: synthesis and its application for the biosorption of Cr (VI) ions from aqueous solution. Desalination Water Treat. 57, 15133–15145.

Mugni, H., Demetrio, P., Paracampo, A., Pardi, M., Bulus, G., Bonetto, C., 2012. Toxicity persistence in runoff water and soil in experimental soybean plots following chlorpyrifos application. Bull. Environ. Contam. Toxicol. 89, 208–212.

Nwosu, F.O., Ajala, O.J., Owoyemi, R.M., Raheem, B.G., 2018. Preparation and characterization of adsorbents derived from bentonite and kaolin clays. Appl. Water Sci. 8, 1–10.

Pashaei-Fakhri, S., Peighambardoust, S.J., Foroutan, R., Arsalani, N., Ramavandi, B., 2021. Crystal violet dye sorption over acrylamide/graphene oxide bonded sodium alginate nanocomposite hydrogel. Chemosphere 270, 129419.

Rana, Kumar, Ashvinder, Frollini, E., Thakur, V.K., 2021. Cellulose nanocrystals: pretreatments, preparation strategies, and surface functionalization. Int. J. Biol. Macromol. 182, 1554–1581. https://doi.org/10.1016/j.ijbiomac.2021.05.119.

Rana, Ashvinder K., Gupta, V.K., Saini, A.K., Voicu, S.I., Abdellattifaand, M.H., Thakur, V.K., 2021a. Water desalination using nanocelluloses/cellulose derivatives based membranes for sustainable future. Desalination 520, 115359. https://doi.org/10.1016/j.desal.2021.115359.

Rana, Ashvinder K., Mishra, Y.K., Gupta, V.K., Thakur, V.K., 2021b. Sustainable materials in the removal of pesticides from contaminated water: perspective on macro to nanoscale cellulose. Sci. Total Environ. 797, 149129. https://doi.org/10.1016/j.scitotenv.2021.149129.

Santos, M.S., Alves, A., Madeira, L.M., 2011. Paraquat removal from water by oxidation with Fenton's reagent. Chem. Eng. J. 175, 279–290.

Sharma, B., Thakur, S., Mamba, G., Prateek Gupta, R.K., Gupta, V.K., Thakur, V.K., 2020a. Titania modified gum tragacanth based hydrogel nanocomposite for water remediation. J. Environ. Chem. Eng. https://doi.org/10.1016/j.jece.2020.104608, 104608.

Sharma, B., Thakur, S., Trache, D., Yazdani Nezhad, H., Thakur, V.K., 2020b. Microwave-assisted rapid synthesis of reduced graphene oxide-based gum tragacanth hydrogel nanocomposite for heavy metal ions adsorption. Nanomaterials 10, 1616.

Tahir, S.S., Rauf, N., 2006. Removal of a cationic dye from aqueous solutions by adsorption onto bentonite clay. Chemosphere 63, 1842–1848.

Thakur, S., Arotiba, O., 2018. Synthesis, characterization and adsorption studies of an acrylic acid-grafted sodium alginate-based TiO2 hydrogel nanocomposite. Adsorpt. Sci. Technol. 36, 458–477.

Thakur, S., Arotiba, O.A., n.d. Synthesis, swelling and adsorption studies of a pH-responsive sodium alginate–poly (acrylic acid) superabsorbent hydrogel. Polym. Bull. 1–20.

Thakur, S., Sharma, B., Verma, A., Chaudhary, J., Tamulevicius, S., Thakur, V.K., 2018. Recent progress in sodium alginate based sustainable hydrogels for environmental applications. J. Clean. Prod. 198, 143–159. https://doi.org/10.1016/j.jclepro.2018.06.259.

Thakur, S., Verma, A., Kumar, V., Jin Yang, X., Krishnamurthy, S., Coulon, F., Thakur, V. K., 2022. Cellulosic biomass-based sustainable hydrogels for wastewater remediation: chemistry and prospective. Fuel 309, 122114. https://doi.org/10.1016/j.fuel.2021.122114.

Thakur, V.K., Thakur, M.K., 2015. Recent advances in green hydrogels from lignin: a review. Int. J. Biol. Macromol. 72, 834–847. https://doi.org/10.1016/j.ijbiomac.2014.09.044.

Thakur, V.K., Voicu, S.I., 2016. Recent advances in cellulose and chitosan based membranes for water purification: a concise review. Carbohydr. Polym. 146, 148–165.

Tsai, W.-T., Lai, C.-W., 2006. Adsorption of herbicide paraquat by clay mineral regenerated from spent bleaching earth. J. Hazard Mater. 134, 144–148.

Verma, A., Thakur, S., Mamba, G., Gupta, R.K., Thakur, P., Thakur, V.K., 2020. Graphite modified sodium alginate hydrogel composite for efficient removal of malachite green dye. Int. J. Biol. Macromol. 148, 1130–1139.

Yue, Y., Wang, X., Wu, Q., Han, J., Jiang, J., 2019. Assembly of polyacrylamide-sodium alginate-based organic-inorganic hydrogel with mechanical and adsorption properties. Polymers 11, 1239.

Zaitan, H., Bianchi, D., Achak, O., Chafik, T., 2008. A comparative study of the adsorption and desorption of o-xylene onto bentonite clay and alumina. J. Hazard Mater. 153, 852–859.

Zare, E.N., Lakouraj, M.M., 2014. Biodegradable polyaniline/dextrin conductive nanocomposites: synthesis, characterization, and study of antioxidant activity and sorption of heavy metal ions. Iran. Polym. J. (Engl. Ed.) 23, 257–266.

Zare, E.N., Lakouraj, M.M., Kasirian, N., 2018. Development of effective nano-biosorbent based on poly m-phenylenediamine grafted dextrin for removal of Pb (II) and methylene blue from water. Carbohydr. Polym. 201, 539–548.

Zare, E.N., Lakouraj, M.M., Mohseni, M., 2014. Biodegradable polypyrrole/dextrin conductive nanocomposite: synthesis, characterization, antioxidant and antibacterial activity. Synth. Met. 187, 9–16.